ACS APPLIED MATERIALS & INTERFACES

Research Article

www.acsami.org

Self-Aligned Formation of Sub 1 nm Gaps Utilizing Electromigration during Metal Deposition

Yasuhisa Naitoh,*,† Tatsuhiko Ohata,‡ Ryuji Matsushita,§ Eri Okawa,‡ Masayo Horikawa,† Makiko Oyama,† Masakazu Mukaida,† Dong F. Wang,*,‡ Manabu Kiguchi,§ Kazuhito Tsukagoshi,∥ and Takao Ishida†

†Nanosystem Research Institute, National Institute of Advanced Industrial Science and Technology (AIST), Namiki 1-2-1, Tsukuba, Ibaraki 305-8564, Japan

‡Micro Engineering & Micro Systems Laboratory, College of Engineering, Ibaraki University, Hitachi, Ibaraki 316-8511, Japan

§Department of Chemistry, Graduate School of Science and Engineering, Tokyo Institute of Technology, 2-12-1 W4-10 Ookayama, Meguro-ku, Tokyo 152-8551, Japan

∥International Center for Materials Architectronics (WPI-MANA), National Institute for Materials Science (NIMS), Tsukuba, Ibaraki 305-0044, Japan

Ⓢ *Supporting Information*

ABSTRACT: We developed a procedure for the fabrication of sub 1 nm gap Au electrodes via electromigration. Self-aligned nanogap formation was achieved by applying a bias voltage, which causes electromigration during metal evaporation. We also demonstrated the application of this method for the formation of nanogaps as small as 1 nm in width, and we found that the gap size can be controlled by changing the magnitude of the applied voltage. On the basis of the electric conductance and surface-enhanced Raman scattering (SERS) measurements, the fabricated gap size was estimated to be nearly equal to the molecular length of 1,4-benzenedithiol (BDT). Compared with existing electromigration methods, the new method provides two advantages: the process currents are clearly suppressed and parallel or large area production is possible. This simple method for the fabrication of a sub 1 nm gap electrode is useful for single-molecule-sized electronics and opens the door to future research on integrated sub 1 nm sized nanogap devices.

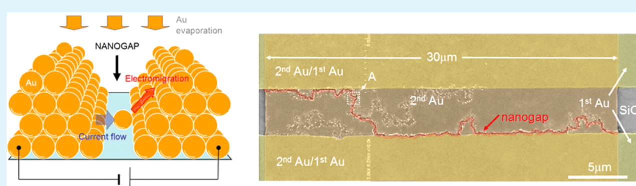

KEYWORDS: *nanogap electrode, electromigration, single-molecule electronics, self-aligned formation, nanogap switch effect, surface-enhanced Raman scattering*

■ INTRODUCTION

Nanogap electrodes consist of two electrodes facing each other across a nanometer-scale separation. They can be used to investigate the electrical properties of nanosized materials, such as molecules and nanoparticles,[1−3] because nanogaps exhibit various characteristic phenomena, such as surface plasmon enhancement, magnetic resistance, nonvolatile memory, and field emission,[4−7] Thus, nanogap electrodes have great potential in nanophotonics and nanoelectronics applications. The characteristic phenomena of nanogap electrodes are dependent on the metal component of the electrodes, the atmosphere, the temperature, the external electrical or magnetic fields, and so on. The gap size is also a factor that influences the characteristics of nanogap electrodes. Therefore, the fabrication of nanogaps with well-defined gap sizes is very important. However, an alternative fabrication process must be developed for the preparation of nanogap devices because the required gap size is much smaller than what is achievable with the current fabrication technology (approximately 22 nm in 2011).[8,9]

Currently, various methods for the preparation of nanogap devices have been studied, including electron beam lithography,[10,11] electroplating,[12] molecular lithography,[13−15] shadow evaporation,[16] and electromigration[17] among others.[18−22] However, on account of the roughness of typical metal films that are fabricated via metal deposition and lift-off processes, a roughness of approximately a few nanometers occurs near the fabricated nanogaps. Therefore, processing with an accuracy of a single nanometer is difficult, and a method that does not require the direct production of the gap via metal deposition is needed.

Electromigration is one of the most popular methods for the fabrication of nanogap electrodes. In this method, nanogap structures are fabricated via electrical breakdown, which involves the passage of an overcurrent through conductive nanowires. Although the fabricated nanogap size is variable, a minimum size of a few nanometers can be achieved.[17] Recently, it was proposed that this electromigration method offers improved fabrication yields, increased control of the nanogap resistance,[23] and enhanced crystallinity of the electrode surface.[24] However, this method suffers from two limitations

Received: July 30, 2013
Accepted: November 26, 2013
Published: November 26, 2013

© 2013 American Chemical Society

dx.doi.org/10.1021/am403115m | ACS Appl. Mater. Interfaces 2013, 5, 12869−12875

with respect to the integration of nanogap devices. First, for high-yield fabrication, careful adjustment of the complicated voltage application while monitoring the conductance changes in the conductive nanowires is necessary.[23] Second, the threshold current for electromigration is very high because it is directly proportional to the cross-sectional area of the conductive nanowire. For example, during the formation of a nanogap on a gold nanowire (45 × 45 nm^2), approximately 1 mA is required for the threshold current.[25] A current of such magnitude may cause damage to the surrounding metal wiring in an integrated circuit.[26] Although the parallel fabrication of 16 nanogaps using the electromigration method has been reported,[27] these two problems remain unaddressed. Recently, our group investigated nonvolatile memory devices using nanogaps mounted on an integrated circuit.[28] To apply the electromigration method to the fabrication of these devices, it was necessary to develop a technique that resolved these issues.

Herein, we present a new method for the fabrication of highly integrated and large electrode area nanogap electrodes. This method involves the application of a voltage to enable simultaneous electromigration and metal deposition during electrode fabrication. Figure 1 shows schematic diagrams of the new method. A constant voltage was applied between prefabricated electrodes, which are illustrated in Figure 1a. During metal deposition, metal islands were initially formed (Figure 1b). As soon as the deposited metal layers were electrically connected to the first electrodes, current flows were concentrated to the metal-bridged parts, and the bridges were removed by electromigration. Metal deposition and electrical breakdown of the metal bridges continuously occurred during the process (Figure 1c). When electromigration sufficiently proceeded to remove all of the bridges, the cross-sectional areas of the removed bridges remained small; thus, nanogap structures were formed with a current lower than that required in previous electromigration methods. Furthermore, the resistance of the nanogaps could be adjusted with that controlling the nanogap electrode, which depended on the magnitude of the applied voltage.[7,29] Because the adjusted resistances reflect the structure of an approximately 1 nm nanogap, it is expected that the new method can achieve the formation of similar-sized gaps. If this assumption is correct, then gap sizes can be automatically controlled without the need for complicated voltage applications; thus, solving the two above-mentioned problems.

In this study, a new electromigration method was investigated. We succeeded in fabricating approximately 1 nm sized Au nanogaps, and their resistance was controlled by adjusting the magnitude of the applied voltage. Moreover, compared with previous methods, the required process currents were considerably smaller, and parallel production was possible. These results indicate that this fabrication method should be applicable to the fabrication of integrated sub 1 nm sized nanogap devices. Fabrication of this sub1 nm sized Au nanogap opens the door to future research in nanospace and nanomaterials in nanospace.

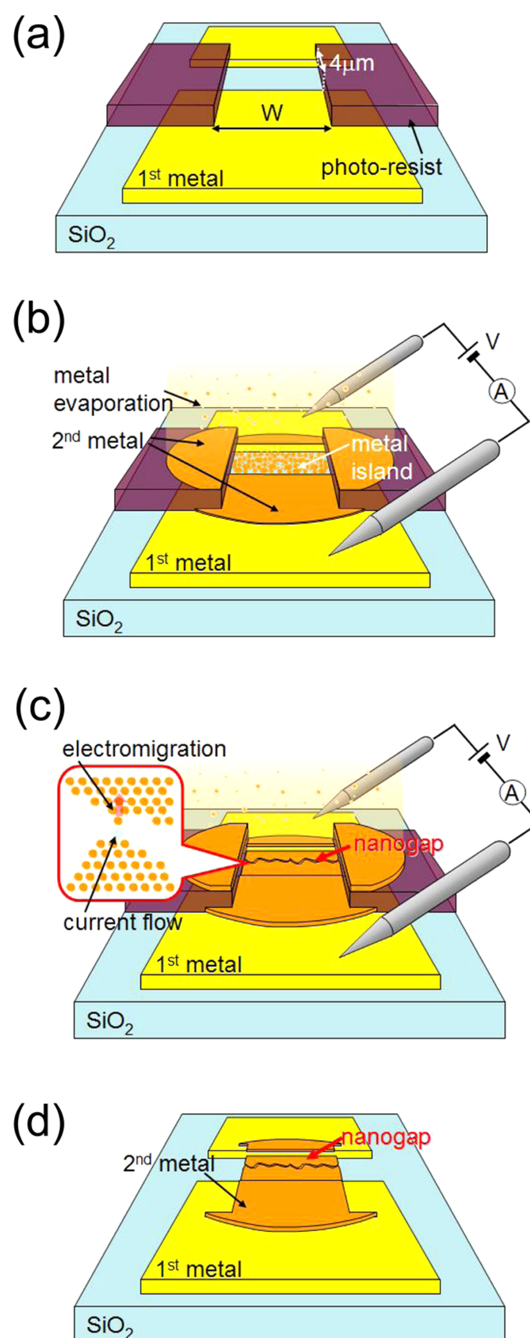

Figure 1. Schematic diagrams of the fabrication procedure. (a) Patterning for the deposition of the second metal by photolithography. (b, c) Second evaporation with the application of voltages and (d) after lift-off.

EXPERIMENTAL SECTION

Nanogap electrodes were prepared by two cycles of photolithography and Au evaporation on a Si substrate covered with a 300 nm thick thermally oxidized layer. Figure 1 shows schematic diagrams of the fabrication process. First, prestructures consisting of 50 nm thick Au electrodes with a 4 μm gap were fabricated. A slit structure with width W was then patterned across the 4 μm gap in the second photolithography step (Figure 1a) followed by the second Au deposition step on the substrate (Figure 1b,c). The width, W, was typically patterned at 30 μm. The deposition was carried out using the thermal evaporator. The deposition rate and film thickness were typically 0.02 nm/s and 20 nm, respectively. During the second deposition step, a voltage was applied for electromigration, and the current was measured using a semiconductor characterization system (Keithley 4200) at room temperature. This applied voltage is referred to as the process voltage. The Au layers have a 1 nm thick Cr layer as an adhesion layer. Figure 1d depicts the fabricated electrodes after lift-off. The fabricated nanogaps were evaluated using field-emission scanning electron microscopy (FESEM) and scanning probe microscopy (SPM; JSPM-5200, JEOL) with a logarithmic current

amplifier. Conductive diamond-coated cantilevers (nanosensors) were used for the SPM measurements. Measurement of electronic properties of nanogap electrodes was carried out using a semiconductor characterization system at room temperature in a vacuum probe station.

The nanogap size was estimated by fitting the data within the range from −1 to 1 V to the tunneling equation given by Simmon's model.[30] The tunneling current is described as follows

$$I = \frac{k_1 A}{G^2}(X^2 \exp(-k_2 G X) - Y^2 \exp(-k_2 G Y)) \quad (1)$$

where $X = (\phi - V/2)^{1/2}$, $Y = (\phi + V/2)^{1/2}$, $k_1 = 6.32 \times 10^{10}$ V s^{-1}, and $k_2 = 1.025$ J$^{-1/2}$. The variables G, A, and ϕ stand for the gap length, the tunneling-emission area, and the barrier height, respectively. To evaluate the nanogap size, the conductivity of 1,4-benzenedithiol (BDT), which has a molecular length of approximately 0.9 nm, was measured using the fabricated nanogap electrodes. The Au nanogap electrodes were immersed in a 1 mM BDT ethanol solution at room temperature for 1 day. After removal of the solution, the I−V characteristics and surface-enhanced Raman scattering (SERS) spectrum[31−34] were measured at room temperature. The I−V characteristics were measured with a semiconductor parameter analyzer at room temperature in a vacuum probe station. The SERS analysis was performed using a commercial Raman microprobe spectrometer with 4 s integrations (Nanofinder30, Tokyo Instruments). Near-infrared (NIR) laser light (λ_{ex} = 785 nm; 70 mW) was used as the excitation light. The NIR beam was focused onto the sample using an objective lens with a 100× magnification and a numerical aperture of 0.95. The estimated spot size of the irradiation was approximately 1 μm.

RESULTS AND DISCUSSION

Figure 2a and its inset graph show the changes in the logarithmic and linear currents, respectively, that accompanied the increase in the Au film thickness when an applied voltage of 0.1 or 10 V was used during the second Au evaporation step (illustrated in Figure 1, panels b and c, respectively). The slit width was 30 μm in this evaporation step. During Cr deposition, which was carried out prior to Au evaporation, the observed currents were below 100 pA, which is the approximate noise level for the equipment. In the early stage of deposition (region I), a rapid increase in the current was observed for both curves. The FESEM image in the inset shows the metal islands on the evaporated film when the current reached 10 nA with an applied voltage of 10 V. The rapid current increase is believed to reflect tunnel current changes that occurred during the growth and connection of the metal islands. Above region I, the current increase became gradual and close to saturation under the influence of internal resistance in the 0.1 V curve. This internal resistance consists of the resistance of the measurement equipment, the contact points between the external wires and electrode pads on the sample substrate, the wiring between the pads and the sample, and so on. This result indicates a change from tunneling conduction to metallic conduction; the current increased as a result of the increase in the cross-sectional area of the metal layers during deposition. Thus, it was concluded that the 0.1 V curve represents a typical metal-deposition process. However, in the 10 V curve and following a large current reduction at the end of region I, the current slightly fluctuated but remained fairly constant with a resistance of approximately 56 kΩ. Because this resistance is greater than the quantum resistance,[35] this result suggests that a nanogap was formed and that current flows removed all of the metal bridges while the current was constant, as shown in Figure 1c. Moreover, the presence of this constant

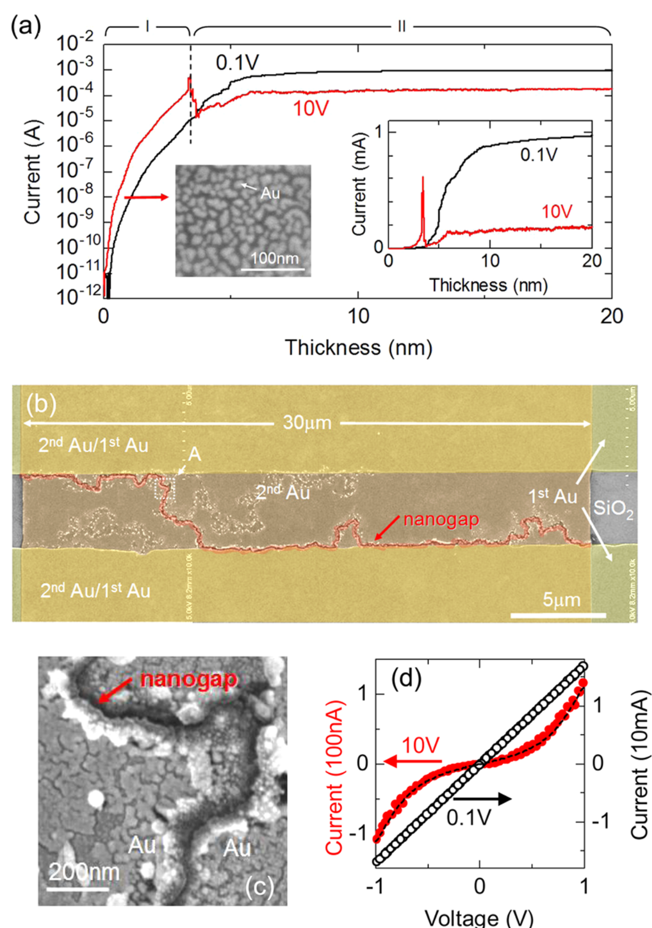

Figure 2. (a) Typical thickness dependence of the logarithmic and linear currents with the application of 0.1 and 10 V. The inset shows the FESEM image of the evaporated film at 1 GΩ in the 10 V curve. (b) FESEM image of the fabricated nanogap electrode with a process voltage of 10 V. The first Au layer, the second Au layer, and the nanogap parts are indicated by the yellow, orange, and red translucent bands, respectively. (c) Magnified FESEM image of the area indicated by the dashed box in panel b. (d) Experimental and fitted I−V curves of samples that were fabricated using process voltages of 0.1 and 10 V.

current indicates that a fixed nanogap was formed in this range by utilizing the resistance controlling the nanogap electrode, which depended on the magnitude of the applied voltage.[7,29] Furthermore, because this constant current was widely observed under various experimental conditions (shown in Figures S2 and S4) with high reproducibility, it can be concluded that constant current is a characteristic of this production method and is an important parameter in nanogap formation. The magnitude of this constant current is referred to as the process current.

The large reduction in the current at the end of region I is also of interest. Within region I, many nanogaps were electrically connected in series between a pair of the first electrodes, as observed in the inset FESEM image. Therefore, the voltage applied to each nanogap was less than the threshold voltage for electromigration of Au atoms.[36,37] The growth and connection of the metal islands thus progressed until the voltage reached the threshold voltage, at which point electromigration suddenly occurred. Therefore, it can be concluded that the large current reduction reflects the threshold value for electromigration. Some steps of current drop were

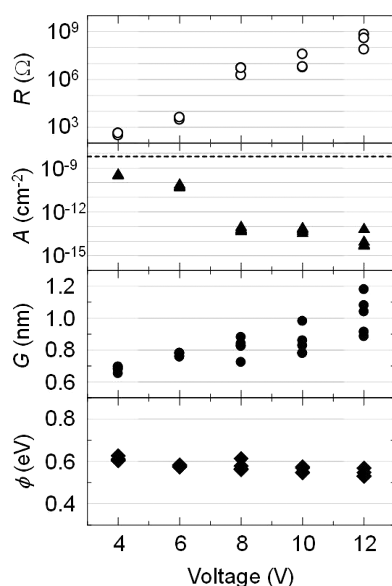

Figure 3. Dependence of the measured resistance at 0.1 V (R), tunneling-emission area (A), gap size (G), and barrier height (ϕ) on the process voltage. A, G, and ϕ were estimated from the fitted $I-V$ curves. The dashed line indicates a 30 μm × 20 nm cross-sectional area as a reference.

observed just after region I. This indicates that some electrical breakdown occurred in this region.

Figure 2b shows the FESEM image of a fabricated sample along with a magnified image of the area indicated by box A in the figure, and the image in Figure 2c shows the nanogap structure surrounding the Au layers, which looks like a valley. In Figure 2b, it can be observed that the nanogap structure was formed like a channel from one end to the other end of the 30 μm wide second Au layer without interruption. This result indicates that the nanogap structure is formed with self-alignment along the entire width. Moreover, structures that appear like tributaries were observed on the second Au layer. Although there is no nanogap structure in these tributaries on the basis of an analysis of the FESEM image, it is assumed that these structures are candidate sites for nanogap formation during the fabrication process. An FESEM image of the sample prepared with an applied voltage of 0.1 V did not show this characteristic channel-like shape of the nanogap.

Next, $I-V$ curves of the fabricated samples were measured and are presented in Figure 2d. The 0.1 V curve shows clear ohmic behavior and a low resistance of approximately 60 Ω, indicating that typical Au deposition occurs during the fabrication process. In contrast, the 10 V curve shows the characteristic $I-V$ shape of tunneling conduction. The estimated gap size G obtained from the fitting of the above-mentioned tunneling equation was approximately 1 nm. This result indicates that the fabrication of approximately 1 nm sized nanogaps can be achieved by this fabrication process. Moreover, resistance switching, which is a characteristic behavior of nanogap electrodes with gaps of less than 10 nm,[7] was observed (Figure S1). This behavior also indicates that the fabricated sample has a nanogap structure.

In Figure 3, the dependence of the resistance (top panel), tunneling-emission area (upper middle panel), gap size (lower middle panel), and barrier height (bottom panel) on the applied voltage is plotted. The resistance was measured at 0.1 V, and the tunneling-emission areas, gap sizes, and barrier heights were estimated via the fitting of the tunneling equation. Five samples were produced for each process voltages ranging from 4 to 12 V. As a result, it was revealed that the resistance increased with increasing process voltage. In addition, from the results of the fitting of the tunneling equation, it was found that the gap size also increased with increasing process voltage. However, the variation in the gap size was approximately 0.2

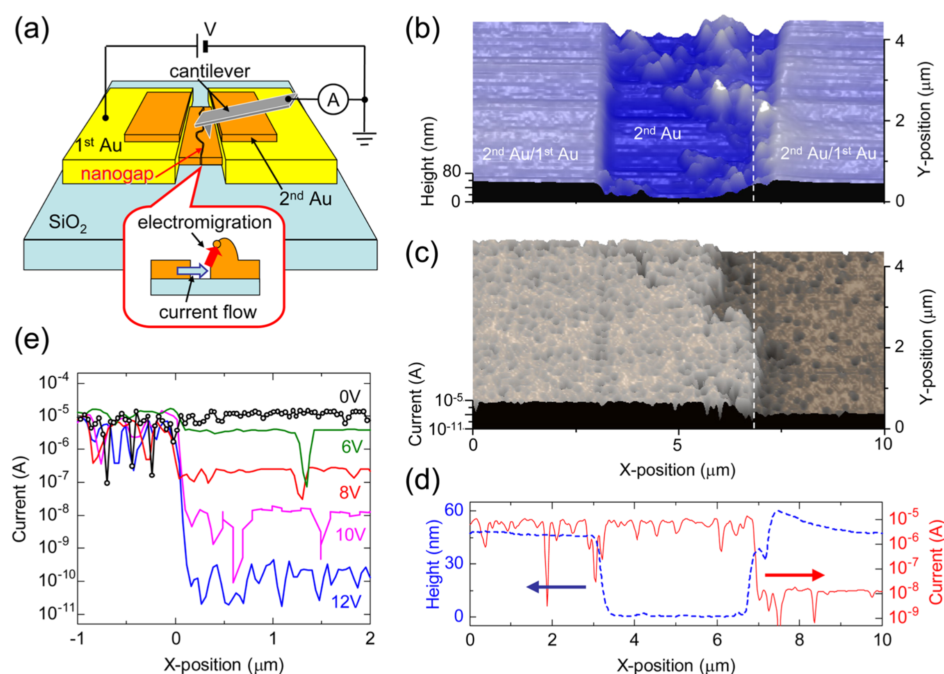

Figure 4. (a) Schematic diagram of the SPM measurement set up. (b) Topographic image, (c) logarithmic current image, and (d) cross-sectional profile of a sample fabricated with a process voltage of 10 V. (e) Cross-sectional profiles of the logarithmic currents of samples fabricated with process voltages of 0, 6, 8, 10, and 12 V.

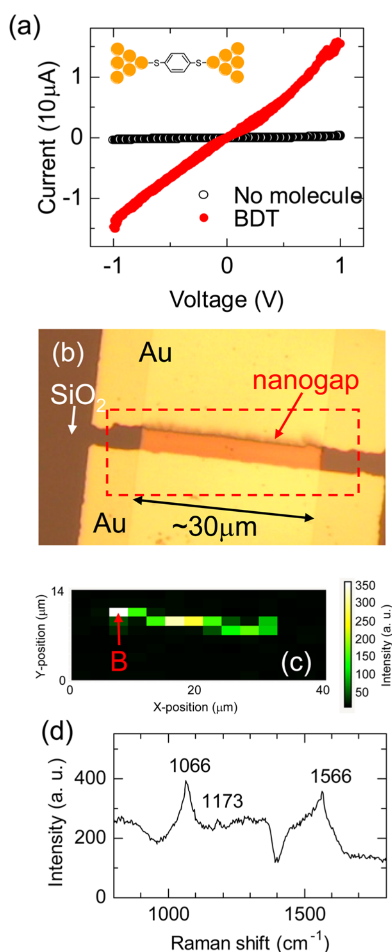

Figure 5. (a) Experimental $I-V$ curves of the Au nanogap electrode before and after the incorporation of bridging BDT molecules. (b) Photograph of the Au nanogap electrode. (c) Map of the BDT SERS signal from the A_1 symmetry mode at 1566 cm^{-1} (integrated from 1500 to 1620 cm^{-1}). (d) Raman spectrum for the site indicated by arrow B in panel c.

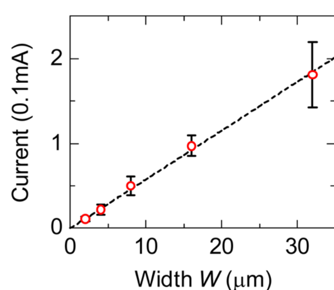

Figure 6. Slit-width dependence of the process current.

nm from 8 to 12 V. The origin of this distribution and methods for improving the control of the gap size are currently under investigation. In addition, although the electrode areas from 8 to 12 V had similar magnitudes, those from 4 to 8 V decreased with increasing process voltage. Furthermore, when the dependence of the current on the thickness at different applied process voltages was investigated (Figure S2), the process currents were found to converge to a steady magnitude at 8, 10, and 12 V but gradually increased in region II at 4 and 6 V. These results indicate that the tunneling-emission areas at 4 and 6 V are simultaneously grown with the formation of the nanogaps and suggest that the fabricated gap size can be controlled by the magnitude of the process voltage, as has been observed for the resistance switching of nanogap electrodes.[7]

The occurrence of electromigration can be confirmed on the basis of the observation of the topographic profile of the nanogap region, as discussed later. The structure of a fabricated sample is shown in Figure 4. Assuming that atom migration occurs via electromigration, then its direction should be the same as that of the electron flow.[38,39] Thus, the migrated atoms should be deposited on the anode side as shown in the inset of Figure 4a, which depicts a block diagram of the SPM measurement. During fabrication, the anodes were located on the right-hand side. A sample voltage of −0.1 V was applied to the left-hand side. Figure 4, panels b−d show the topographic image, logarithmic current image, and cross-sectional profile, respectively, of a sample fabricated using a process voltage of 10 V. The anode in the fabrication process is on the right-hand side in the images. The images in Figure 4b,c were simultaneously observed; the dashed lines indicate the same position. The nanogap structures could not be directly observed in the topographic image. However, a sharp drop in current was observed at X = 6 to 7 μm in Figure 4c; this drop corresponds to the position of the nanogap. Figure 4e shows the cross-sectional profile of the logarithmic currents of samples fabricated with various applied process voltages. In the figure, similar sharp drops were observed for these samples, whereas gradual changes were not observed. This result indicates that the resistance in these samples originated from a single nanogap and not from a series of nanogaps. Comparing the left- and right-hand sides of the profile in Figure 4d near the nanogap, it can be observed that the right-hand side was raised, which also suggests that the deposition of migrated atoms occurred during electromigration, as mentioned earlier.

Next, to confirm that the fabricated nanogap was about 1 nm in size, the bridging structure was investigated using BDT, which has a molecular length of approximately 0.9 nm. Figure 5a presents the $I-V$ curves before and after immersion in a BDT solution. The resistance of the as-fabricated sample was 12 MΩ at 0.1 V (gap size of approximately 0.9 nm) and decreased to 78 kΩ after immersion. Given that a single BDT molecule has a conductivity ranging from 8.6 to 850 nS,[40−42] the change in the resistance indicates that approximately 15 to 1500 BDT molecules were bridged in the nanogap. The location of the BDT molecules adsorbed on the nanogap can be imaged by mapping the SERS signal. Figure 5b shows an optical microscopy image of the sample after bridging, and Figure 5c shows a map of the BDT SERS signal from the A_1 symmetry mode at 1566 cm^{-1} (integrated from 1500 to 1620 cm^{-1}), as marked by the dashed box in Figure 5b. The Raman spectrum of the site indicated by arrow B in Figure 5c is presented in Figure 5d. The spectrum shows typical signals at 1066, 1173, and 1566 cm^{-1}, which are assigned to C−C stretching, C−H bending, and C=C stretching modes, respectively.[31] These SERS signals were enhanced by the Au nanogap, indicating that the BDT molecules are bridged between the Au electrodes, with the bright spots in the map indicating the bridged BDT positions. The spots can be observed for a length of approximately 30 μm, providing evidence that a relatively uniform gap with a sub 1 nm width and a length of 30 μm was created.

Figure 6 illustrates the relationship between the process current at 10 V and the slit width, W, which was varied from 2 to 32 μm. Each point was estimated as the average of

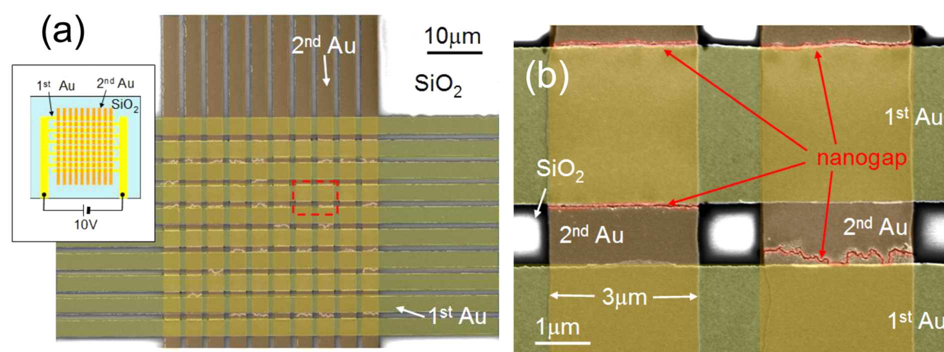

Figure 7. (a) FESEM image and schematic diagram of a 9 × 10 parallel nanogap electrode. (b) Magnified image of the area indicated by the dashed box in panel a. The first Au layer, the second Au layer, and the nanogap parts are indicated by the yellow, orange, and red translucent bands, respectively.

measurements for five samples. (Variation in the current as a function of the thickness at different slit widths can be observed in Figure S4). As can be observed in Figure 6, the process current was proportional to the slit width, which indicates that the nanogaps are somewhat uniformly distributed in the slit. Therefore, although there is some distribution of the nanogap size at fixed applied voltages (Figure 3), the process results in the fabrication of uniform nanogaps in parallel via electromigration during evaporation. Moreover, current density, estimated from the slope of the line in Figure 6, was 2.6×10^8 A/m^2; this value is less than one thousandth of that required for typical electromigration processes.[25] This current reduction is a strong advantage for electromigration during metal deposition and thus this process is expected to be applicable to the production of large area and integrated sub 1 nm sized nanogap devices.

The FESEM image of a nanogap electrode with parallel nanogap structures is shown in Figure 7a, and a magnified image of the area indicated by the dashed box in Figure 7a is shown in Figure 7b. The first Au layer was deposited as a pair of interdigitated electrodes with five fingers each (yellow part in the inset of Figure 7). The second Au layer was deposited as 10 strips in a direction perpendicular to the first layer (brown part in the inset of Figure 7). During the second Au deposition step, a process voltage of 10 V was applied between the pair of interdigitated Au electrodes. After close inspection of the FESEM image, it was concluded that the formation of nanogap structures was achieved in all of the 9 × 10 sections without the fatal destruction that could be caused by overcurrent flows. Many nanogaps were formed near the edge of the first Au layer when the electrode width, *W*, was small, suggesting that the first nanogap was formed on the edge under the influence of the shadow of the first Au layers during the second layer deposition. Remarkably, the process current remained below a few milliamperes during the formation of all 90 nanogaps; the achievement of a very-low-current electromigration method was thus demonstrated. This result indicates that a large number of nanogaps can be simultaneously fabricated in parallel by our fabrication method.

■ CONCLUSIONS

We successfully developed a new nanogap fabrication method in which a voltage is simultaneously applied with metal deposition, inducing the concurrent electromigration of the metals. We also demonstrated the application of this method for the formation of nanogaps as small as 1 nm in width and found that the gap size can be controlled by changing the magnitude of the applied voltage. Compared with existing methods, the new method provides two advantages: the process current densities are smaller and parallel production is possible. Importantly, this fabrication method is applicable to the preparation of large area and integrated sub 1 nm sized nanogap devices.

■ ASSOCIATED CONTENT

Supporting Information

Electrical properties for resistance switching using a fabricated sample, dependence of the current on the thickness at various voltages, FESEM images, and the dependence of the current on the thickness at various slit widths during the second Au evaporation step. This material is available free of charge via the Internet at http://pubs.acs.org.

■ AUTHOR INFORMATION

Corresponding Authors

*E-mail: ys-naitou@aist.go.jp (Y.N.).
*E-mail: dfwang@mx.ibaraki.ac.jp (D.W.).

Notes

The authors declare no competing financial interest.

■ ACKNOWLEDGMENTS

T.I. and M.O. acknowledge financial support from the Japan Society for the Promotion of Science (JSPS) for a Grant-in-Aid for Scientific Research (no. 24310083). The authors extend their deep appreciation to Mr. Y. Masuda, Mr. S. Furuta, Mr. T. Takahashi, and Dr. M. Ono of Funai Electronics Advanced Applied Technology Research Institute, Inc. for their advice on a wide range of issues regarding this study. The fabrication of materials in this study was partly supported by the AIST Nano-Processing Facility (NPF). We also thank Enago and Dr. N. Minami (Advanced Industrial Science and Technology, AIST) for the English language review.

■ REFERENCES

(1) Bezryadin, A.; Dekker, C.; Schmid, G. *Appl. Phys. Lett.* **1997**, *71*, 1273−1275.
(2) Song, H.; Reed, M. A.; Lee, T. *Adv. Mater.* **2011**, *23*, 1583−1608.
(3) Suga, H.; Naitoh, Y.; Tanaka, M.; Horikawa, M.; Kobori, H.; Shimizu, T. *Appl. Phys. Express* **2009**, *2*, 055004-1−055004-3.
(4) Pile, D. F. P.; Ogawa, T.; Gramotnev, D. K.; Matsuzaki, Y.; Vernon, K. C.; Yamaguchi, K.; Okamoto, T.; Haraguchi, M.; Fukui, M. *Appl. Phys. Lett.* **2005**, *87*, 261114-1−261114-3.

(5) Céspedes, O.; Clifford, E.; Coey, J. M. D. *J. Appl. Phys.* **2005**, *97*, 064305-1−064305-6.
(6) Fujii, H.; Kanemaru, S.; Hiroshima, H.; Gorwadkar, S. M.; Matsukawa, T.; Itoh, J. *Appl. Surf. Sci.* **1999**, *146*, 203−208.
(7) Naitoh, Y.; Horikawa, M.; Abe, H.; Shimizu, T. *Nanotechnology* **2006**, *17*, 5669−5674.
(8) Borghetti, J.; Snider, G. S.; Kuekes, P. J.; Yang, J. J.; Stewart, D. R.; Williams, R. S. *Nature* **2010**, *464*, 873−876.
(9) Pershin, Y. V.; Ventra, M. Di *Adv. Phys.* **2011**, *60*, 145−227.
(10) Saifullah, M. S. M.; Ondarçuhu, T.; Koltsov, D. K.; Joachim, C.; Welland, M. E. *Nanotechnology* **2002**, *13*, 659−662.
(11) Guillorn, M. A.; Carr, D. W.; Tiberio, R. C.; Greenbaum, E.; Simpson, M. L. *J. Vac. Sci. Technol., B* **2000**, *18*, 1177−1181.
(12) Morpurgo, A. F.; Marcus, C. M.; Robinson, D. B. *Appl. Phys. Lett.* **1999**, *74*, 2084−2086.
(13) Tanaka, H.; Anderson, M. E.; Horn, M. W.; Weiss, P. S. *Jpn. J. Appl. Phys.* **2004**, *43*, L950−L953.
(14) Anderson, M. E.; Mihok, M.; Tanaka, H.; Tan, L. P.; Horn, M. W.; McCarty, G. S.; Weiss, P. S. *Adv. Mater.* **2006**, *18*, 1020−1022.
(15) Jiang, L.; Dong, H.; Meng, Q.; Tan, J.; Jiang, W.; Xu, C.; Wang, Z.; Hu, W. *Adv. Mater.* **2012**, *24*, 694−698.
(16) Naitoh, Y.; Tukagoshi, K.; Murata, K.; Mizutani, W. *e-J. Surf. Sci. Nanotechnol.* **2003**, *1*, 41−44.
(17) Park, H.; Lim, A. K. L.; Alivisatos, A. P.; Park, J.; McEuen, P. L. *Appl. Phys. Lett.* **1999**, *75*, 301−303.
(18) Gao, P.; Zhang, Q.; Li, H.; Chan-Park, M. B. *Small* **2011**, *7*, 2195−2200.
(19) Tian, X.; Li, J.; Xu, D. *Electrochem. Commun.* **2010**, *12*, 1081−1083.
(20) Yasutake, Y.; Kono, K.; Kanehara, M.; Teranishi, T.; Buitelaar, M. R.; Smith, C. G.; Majima, Y. *Appl. Phys. Lett.* **2007**, *91*, 203107-1−203107-3.
(21) Li, T.; Hu, W.; Zhu, D. *Adv. Mater.* **2010**, *22*, 286−300.
(22) Valladares, L. D. L. S.; Felix, L. L.; Dominguez, A. B.; Thanos Mitrelias, T.; Sfigakis, F.; Khondaker, S. I; Barnes, C. H. W.; Majima, Y. *Nanotechnology* **2010**, *21*, 445304-1−445304-8.
(23) Strachan, D. R.; Smith, D. E.; Johnston, D. E.; Park, T.-H.; Therien, M. J.; Bonnell, D. A.; Johnson, A. T. *Appl. Phys. Lett.* **2005**, *86*, 043109-1−043109-3.
(24) Suga, H.; Sumiya, T.; Furuta, S.; Ueki, R.; Miyazawa, Y.; Nishijima, T.; Fujita, J.; Tsukagoshi, K.; Shimizu, T.; Naitoh, Y. *ACS Appl. Mater. Interfaces* **2012**, *4*, 5542−5546.
(25) Durkan, C.; Schneider, M. A.; Welland, M. E. *J. Appl. Phys.* **1999**, *86*, 1280−1286.
(26) Hau-Riege, C. S. *Microelectron. Reliab.* **2004**, *44*, 195−205.
(27) Johnston, D. E.; Strachan, D. R.; Johnson, A. T. C. *Nano Lett.* **2007**, *7*, 2774−2777.
(28) Takahashi, T.; Furuta, S.; Masuda, Y.; Kumaragurubaran, S.; Sumiya, T.; Ono, M.; Hayashi, Y.; Shimizu, T.; Suga, H.; Horikawa, M.; Naitoh, Y. Silicon Nanoelectronics Workshop (SNW), 2012 IEEE, Honolulu, HI, June 10−11, 2012; DOI: 10.1109/SNW.2012.6243334.
(29) Masuda, Y.; Takahashi, T.; Furuta, S.; Ono, M.; Shimizu, T.; Naitoh, Y. *Appl. Surf. Sci.* **2009**, *256*, 1028−1030.
(30) Simmons, J. G. *J. Appl. Phys.* **1963**, *34*, 2581−2590.
(31) Tian, J. H.; Liu, B.; Li, X.; Yang, Z. L.; Ren, B.; Wu, S. T.; Tao, N.; Tian, Z. Q. *J. Am. Chem. Soc.* **2006**, *128*, 14748−14749.
(32) Liu, Z.; Ding, S. Y.; Chen, Z.-B.; Wang, X.; Tian, J. H.; Anema, J. R.; Zhou, X. S.; Wu, D. Y.; Mao, B. W.; Xu, X.; Ren, B.; Tian, Z. Q. *Nat. Commun.* **2011**, *2*, 1310-1−1310-6.
(33) Ioffe, Z.; Shamai, T.; Ophir, A.; Noy, G.; Yutsis, I.; Kfir, K.; Cheshnovsky, O.; Selzer, Y. *Nat. Nanotechnol.* **2008**, *3*, 727−732.
(34) Matsuhita, R.; Horikawa, M.; Naitoh, Y.; Nakamura, H.; Kiguchi, M. *J. Phys. Chem. C* **2013**, *117*, 1791−1795.
(35) Agraita, N.; Yeyati, A. L.; Ruitenbeek, J. M. *Phys. Rep.* **2003**, *377*, 81−279.
(36) Umeno, A.; Hirakawa, K. *Appl. Phys. Lett.* **2009**, *94*, 162103-1−162103-3.
(37) Suga, H.; Horikawa, M.; Odaka, S.; Miyazaki, H.; Tsukagoshi, K.; Shimizu, T.; Naitoh, Y. *Appl. Phys. Lett.* **2010**, *97*, 073118-1−073118-3.
(38) Bondarchuk, O.; Cullen, W. G.; Degawa, M.; Williams, E. D.; Bole, T.; Rous, P. J. *Phys. Rev. Lett.* **2007**, *99*, 206801-1−206801-4.
(39) Girod, S.; Bubendorff, J.-L.; Montaigne, F.; Simon, L.; Lacour, D.; Hehn, M. *Nanotechnology* **2012**, *23*, 365302-1−365302-4.
(40) Haiss, W.; Wang, C.; Jitchati, R.; Grace, I.; Martín, S.; Batsanov, A. S.; Higgins, S. J.; Bryce, M. R.; Lambert, C. J.; Jensen, P. S.; Nichols, R. J. *J. Phys.: Condens. Matter* **2008**, *20*, 374119-1−374119-9.
(41) Xiao, X.; Xu, B.; Tao, N. *Nano Lett.* **2004**, *8*, 267−271.
(42) Taniguchi, M.; Tsutsui, M.; Yokota, K.; Kawai, T. *Nanotechnology* **2009**, *20*, 434008-1−434008-8.